SCIENTIFIC REPORTS

OPEN

# Magneto-active substrates for local mechanical stimulation of living cells

Received: 4 April 2017
Accepted: 27 December 2017
Published online: 23 January 2018

Cécile M. Bidan[1], Mario Fratzl[2,3], Alexis Coullomb[1], Philippe Moreau[1], Alain H. Lombard[1], Irène Wang[1], Martial Balland[1], Thomas Boudou[1], Nora M. Dempsey[2], Thibaut Devillers[2] & Aurélie Dupont[1]

**Cells are able to sense and react to their physical environment by translating a mechanical cue into an intracellular biochemical signal that triggers biological and mechanical responses. This process, called mechanotransduction, controls essential cellular functions such as proliferation and migration. The cellular response to an external mechanical stimulation has been investigated with various static and dynamic systems, so far limited to global deformations or to local stimulation through discrete substrates. To apply local and dynamic mechanical constraints at the single cell scale through a continuous surface, we have developed and modelled magneto-active substrates made of magnetic micro-pillars embedded in an elastomer. Constrained and unconstrained substrates are analysed to map surface stress resulting from the magnetic actuation of the micro-pillars and the adherent cells. These substrates have a rigidity in the range of cell matrices, and the magnetic micro-pillars generate local forces in the range of cellular forces, both in traction and compression. As an application, we followed the protrusive activity of cells subjected to dynamic stimulations. Our magneto-active substrates thus represent a new tool to study mechanotransduction in single cells, and complement existing techniques by exerting a local and dynamic stimulation, traction and compression, through a continuous soft substrate.**

Living cells have a sense of touch, which means that they are able to feel, respond and adapt to the mechanical properties of their environment. The process by which cells convert mechanical signals into biochemical signals is called mechanotransduction. Defects in the mechanotransduction pathways are implicated in numerous diseases ranging from atherosclerosis and osteoporosis to cancer progression and developmental disorders[1,2]. Since the 1990s, different static studies focused on mechanosensing have shown that cells can migrate along the rigidity gradient direction[3] and that stem cells can differentiate *in vitro* according to their substrate's stiffness[4] and geometry[5]. The interplay between a mechanical force and the reinforcement of cell adhesion has also been documented[6,7]. In their natural environment, cells face a complex and dynamic mechanical environment. Cyclic strain can induce reorientation of adherent cells and affect cell growth depending on the temporal and spatial properties of the mechanical stimulation[8–11]. The relevant timescales span from the milli-second for the stretching of mechanosensitive proteins, minutes for mechanotransduction signalling to hours for global morphological changes and even longer for adapting cell functions[12]. Taken together, previous works have shown that cells are sensitive to both the spatial and temporal signatures of mechanical stimuli. In order to study mechanotransduction, it is thus essential to stimulate cells with mechanical cues controlled both spatially and temporally.

To address this topic, various methods have been proposed to exert experimentally controlled mechanical stimuli on adherent cells[13]. For instance, local stimuli were applied by direct contact with an AFM tip[14], or with microbeads adhering on the cell membrane and actuated by magnetic[15] or optical tweezers[16]. Although local enough to address the subcellular mechanisms of mechanotransduction, these methods involve intrinsic perturbations of the cell structure through mechanical interactions with a stiff object of fixed geometry. Cell stretchers were developed to induce mechanical stimulation via substrates of tunable substrate rigidity[8,17]. Despite being more physiological and less invasive, such approaches only enable global deformation at the cellular scale. To

[1]University Grenoble Alpes, CNRS, LIPhy, 38000, Grenoble, France. [2]University Grenoble Alpes, CNRS, Grenoble INP, Institut Néel, 38000, Grenoble, France. [3]University Grenoble Alpes, CNRS, Grenoble INP, G2Elab, 38000, Grenoble, France. Correspondence and requests for materials should be addressed to T.D. (email: thibaut.devillers@neel.cnrs.fr) or A.D. (email: aurelie.dupont@univ-grenoble-alpes.fr)

get around this limitation, different geometries of vertical indenters were used to impose various deformation patterns on soft continuous cell substrates[18]. Surfaces made of micropillars that can be actuated with a magnetic field were proposed to apply local and dynamic mechanical stimuli[19–21] but such discrete surfaces can affect the cellular behaviour[22,23].

Interestingly, only one of these systems was used to apply compression on single cells[21]. Yet, compressive stress is present in healthy tissue such as cartilage[24,25] and is crucial during embryonic development[26]. A compressive stress has also been shown to alter tumour growth and shape *in vitro*[27–29] which seems relevant *in vivo* where tumours have to grow against surrounding tissue. Most of the studies on compressive stress have been carried out at the tissue or multicellular level. There is currently a lack of studies at the single cell scale, required to understand the possible differences in the mechanotransduction response between traction and compression stresses.

In this article, we propose a new method to produce deformable substrates that enable local and dynamic mechanical stimulation of cells plated on a continuous surface. These substrates consist of iron micro-pillars spatially arranged in a soft elastomer and locally actuated using a magnetic field generated by two electromagnets. Localized deformation of the substrate is controlled through the current input to the coils of the electromagnet and is quantified by tracking fluorescent markers incrusted under the surface of the elastomer. Traction force microscopy (TFM) is used to estimate the magnitude of stress generated by the pillar on the surface, which is in the range of the typical stress applied by contractile cells. Stress variation graphs demonstrate that cells spread on the magneto-active substrates can be mechanically stimulated both in tension and in compression. Live TFM of an exemplary cell stimulated by a magnetic pillar is also demonstrated. Finally, a proof of principle experiment on living cells is presented, showing increased protrusive activity of fibroblasts after a period of mechanical stimulation.

The present approach allows the stimulation of living cells with deformation patterns controllable in space and time. The magneto-active substrates can be deformed continuously at the single cell scale both in traction and compression while the inherent coupling with TFM allows to map the corresponding stresses. Thanks to their compatibility with standard fluorescence techniques, these magneto-active substrates pave the way to quantitative studies of intracellular biochemical responses resulting from controlled mechanical stimulations.

## Methods

The active substrates developed in this work consist of an array of magnetic micro-pillars embedded in a continuous layer of soft polydimethylsiloxane (PDMS). Upon application of a magnetic field generated by two electromagnets, the micro-pillars are slightly tilted, resulting in the local deformation of the surface of the PDMS. This section describes the methods used to produce and characterize the micro-pillars and the substrates as well as the protocols to actuate the magneto-active substrates for live-cell experiments (Fig. 1).

**Microfabrication of magnetic micro-pillars and magnetic templates.** The micro-pillars consist of cylindrical silicon cores coated with a shell of soft magnetic iron (Fe). The silicon pillars were produced by etching the surface of a silicon wafer according to the following procedure. A network of 10 µm diameter disks of S1818 resin was produced on a silicon wafer by standard optical lithography. The silicon wafer was then etched over 30 µm using deep reactive ion etching (DRIE) following the Bosch process. The resin acts as a mask, as the much higher rate of etching of the silicon compared to the resin results in the formation of a dense array of silicon pillars which are 30 µm in height and 10 µm in diameter (Fig. 1A). The remaining resin is then dissolved in acetone, and the substrate cleaned with an $O_2$ plasma to remove residual organic traces.

The entire wafer surface was covered with a trilayer of Ta(100 nm)/Fe(10 µm)/Ta(100 nm) deposited by triode sputtering at room temperature under a base pressure of $10^{-6}$ mbar according to a procedure described elsewhere[30]. The role of the tantalum (Ta) is to protect the iron from oxidation. The deposition by triode sputtering is relatively directive, so that the layer deposited on the top of the pillar and on the substrate between pillars is thicker than the layer deposited on the sidewalls of the pillars, as shown in the focused ion beam cut of a pillar in Fig. 1A. The pillars were mechanically detached from the substrate by swiping the surface of the patterned substrate with a glass coverslip within a bath of absolute ethanol. The micro-pillars from a known surface area were then air dried and stored in 5 mL tubes for later use.

Using the magnetic field gradient force, it is possible to organize the magnetic micro-pillars inside PDMS, to favour a particular spatial arrangement[31]. For this purpose, we produced a magnetic template using the approach described above (patterning of a Si substrate using DRIE followed by film deposition). As a template, 50 µm wide Si stripes separated by 500 µm were produced at the surface of a Si substrate and Ta(100 nm)/Fe(10 µm)/Ta(100 nm) was deposited on the substrate using triode sputtering. The application of an external magnetic field, produced by a macroscopic permanent magnet positioned below the template, served to magnetize the Fe micro-stripes. The strong magnetic field gradients produced by the micro-stripes of the template attract the magnetic micro-pillars, inducing an organization of the pillars along parallel lines in the PDMS. The stray field of the bulk magnet serves to align the long axis of the micro-pillars out of the plane of the substrate.

**Magneto-active substrate fabrication.** PDMS base and crosslinker from a standard kit (Sylgard 184, Dow Corning) were mixed in the respective mass proportions 40:1. To reach a softer but non-sticky matrix, 8 parts of silicone oil (50 cSt, 378356, Sigma) were added. After stirring thoroughly, the mixture was degassed for 20 min and then 1 mL of the mixture was added into tubes containing about $8{\cdot}10^4$ pillars. After stirring thoroughly in each tube, the PDMS/pillar mixtures were degassed for 1 h. Carboxylate-modified fluorescent beads (dark red FluoSpheres® 660/680, 0.2 µm, Life Technologies) were diluted 1:500 in isopropanol and sonicated for 3 minutes. 50 µL of bead solution were spread with a pipette tip on 35 × 35 mm squares of 50 µm thick polypropylene sheet (PP301351/1, Goodfellow), the excess was removed and the isopropanol was then air dried.

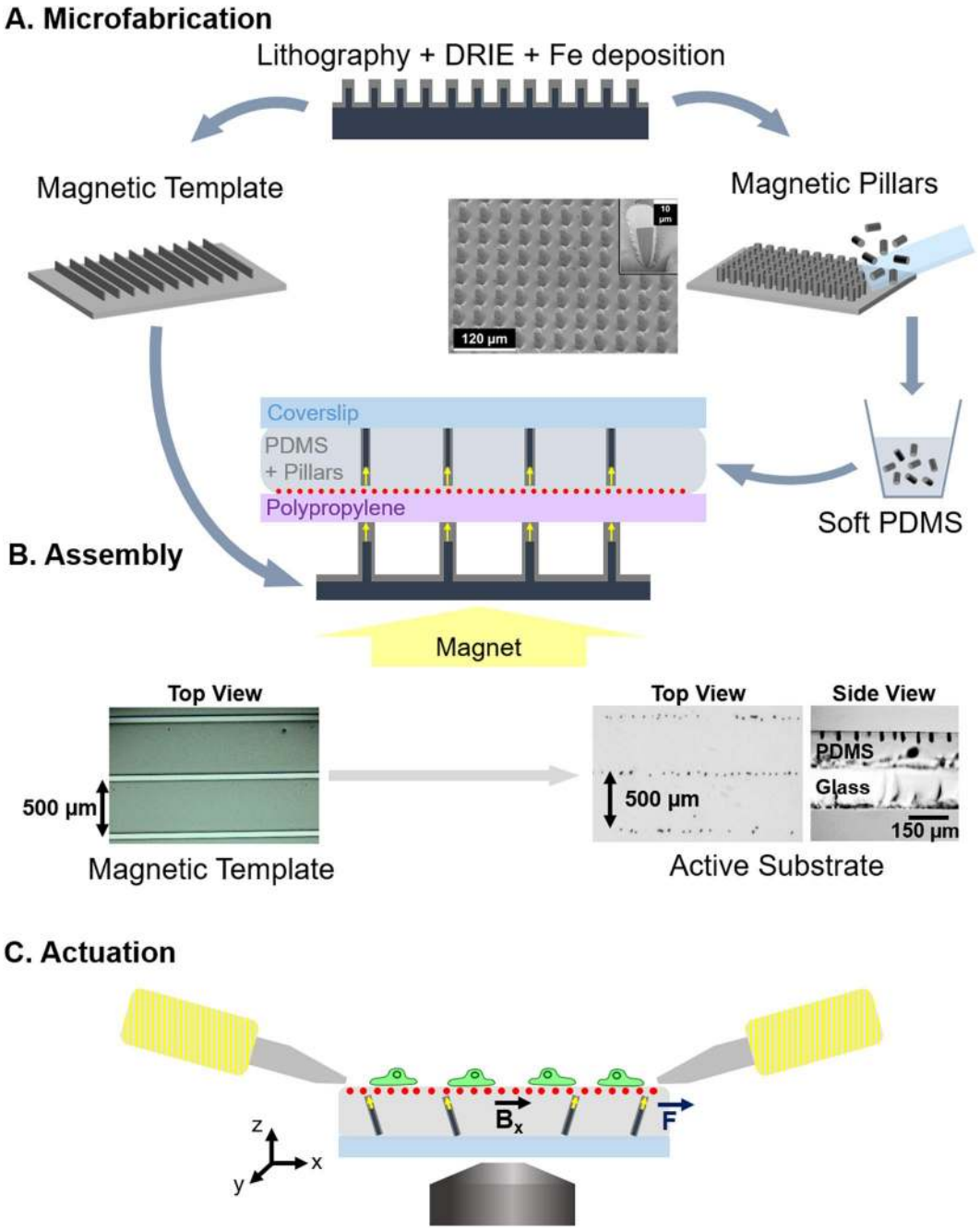


**Figure 1.** Experimental workflow. (**A**) Magnetic micro-pillars and template are made by optical lithography followed by deep reactive ion etching (DRIE) and iron deposition by sputtering. The magnetic pillars are mechanically detached from the wafer and mixed with soft PDMS prior to casting between a sheet of polypropylene coated with fluorescent beads and a coverslip. (**B**) The resulting sandwich structure is positioned on a magnetic template laid on a large permanent magnet, so as to align the pillars vertically (side view) and organize them according to the pattern of the template (top view). (**C**) After peeling off the polypropylene sheet, coating the surface with proteins and plating cells on the top, the substrates are placed in the magnetic field generated by two electromagnets so as to actuate the pillars via a magnetic torque. The actuation setup is mounted on a microscope to quantify the local deformation of the surface by tracking the fluorescent beads and to follow the response of the cells to the mechanical stimulation.

To assemble the magneto-active substrate, 120 µL of PDMS/pillar mixture was poured on each polypropylene square and carefully covered with a 32 mm coverslip to avoid the inclusion of bubbles. To orient and organize the micro-pillars in the substrate, the stack was positioned over the magnetic template on a large permanent magnet (60 mm diameter, Supermagnete) as shown in Fig. 1B. The ensemble was kept at 65 °C overnight to cure the PDMS and then the magneto-active substrates were stored at room temperature in the dark. Before use for cell

culture, the polypropylene sheet was carefully removed and a 26 mm silicone ring activated with $O_2$ plasma was stuck on the PDMS surface to confine cells and culture medium.

**Magnetic field source for actuation on the microscope stage.** A pair of electromagnets were made by winding 1 mm diameter copper wire around 10 cm long aluminium tubes, i.e. 250 turns over 2.5 layers. Magnetically soft iron pole pieces were used to focus the magnetic field 2 cm away from the coil and their tips were shaped as a bevel (30° on one side, 13° on the other side). The coils were plugged in series on a current generator ($I_{max} = 9$ A). The pair of electromagnets was mounted on the stage of an epifluorescence microscope equipped with a chamber maintained at 37 °C to enable live cell imaging. Before cell experiments, the tips of the electromagnet pole pieces were wrapped in a thin film of Teflon to prevent sticking on the surface of the substrate and rusting of the pole pieces (soft iron).

**Characterization methods.** The magnetic field generated in between the electromagnets was estimated macroscopically with a Hall probe (Allegro A1302, Microsystem Inc.). The magnetic moment of individual pillars was calculated from the magnetic moment of a population of about $8{\cdot}10^4$ pillars measured using an extraction magnetometer.

The average dimensions of the magnetic pillars after collection were estimated from the measurement of 39 pillars with a bright field microscope.

The average thickness of the substrate was measured optically on samples containing fluorescent beads at both interfaces of the PDMS. To assess the local mechanical properties of the magneto-active substrates, force-indentation profiles were performed in 1% Pluronic diluted in PBS at a frequency of 1 Hz using an atomic force microscope BioCatalyst (Bruker) equipped with borosilicate sphere-tipped cantilevers of radius $R = 2.5$ µm (Novascan Technologies) and a spring constant of 0.4 N/m. Young's moduli were calculated by least-square fitting of the experimental force indentation curves using NanoScope Analysis (Bruker). Soft PDMS patches of 20 mm diameter and 2 mm thickness were also produced to measure the global viscoelastic properties (shear storage modulus G′ and loss modulus G″) of the substrate with a rheometer (Bohlin) used in parallel plane geometry at deformation amplitudes $\gamma$ varied between 0.01% and 20% of shear and frequencies varied between 0.01 Hz and 10 Hz.

**Numerical modelling.** In a simple approximation, the present system can be considered as a network of elongated magnets which experience a torque due to the application of a transverse (in-plane) magnetic field. Numerical modelling was performed using COMSOL Multiphysics 5.0 (COMSOL Group, Stockholm, Sweden) in order to define the limits of this simplistic approach and understand the parameters which are relevant to the dimensioning of the system. All simulations were performed on a Dell OptiPlex 9020 (Dell Inc., Round Rock, TX.) powered with an Intel Core i5 4$^{th}$ generation/3.3 GHz (Intel Corporation, Santa Clara, Ca.).

In a first simulation, the magnetic field distribution produced by the electromagnets was modelled in 2D (i.e. in the x-z plane bisecting the electromagnets' pole pieces, where x is in the plane of the substrate and z is out of the substrate plane – see Fig. 1C). As the magnetic field source, we considered the magnetic pole pieces of the electromagnets, and used as input their real geometry with a distance of 6 mm between the poles' apex. To reduce the computational load, the electromagnets were modelled as permanent magnets, homogeneously magnetized along their axis. Their magnetization was adjusted in such a way that the theoretical value of the generated field's projection along the horizontal direction ($B_x$) matches the experimental values measured in the centre of the system for a current of 5 A.

A second model was developed to analyse quantitatively the magnetic and mechanical response of a single pillar in PDMS when exposed to an external magnetic field. In this 3D magneto-mechanical model, the pillar was represented as a cylinder of silicon, with a diameter of 10 µm and a height of 25 µm. The Fe shell is 2 µm thick on the sidewalls and 10 µm thick on the top of the pillar. The relative permeability of iron was taken as $\mu_r = 5000$. The PDMS film is 115 µm thick, with the top of the pillar being 1 µm below the PDMS surface. The top surface of PDMS is described as a free surface while the bottom one is mechanically attached to the glass substrate. The PDMS was approximated as a linear elastic material, with a Young's modulus $E = 20.3$ kPa and a shear modulus $G = 7.1$ kPa as estimated experimentally.

**Cells.** The magneto-active substrates were sterilized in 70% ethanol for at least 20 min and rinsed with PBS before use. The surface was then incubated for 1 h in 20 µg/mL fibronectin (Sigma) solution diluted in PBS, a disk of Teflon was used to spread the fibronectin drop on the hydrophobic surface. The substrate was rinsed with PBS and conditioned with culture medium at 37 °C for at least 30 min.

These substrates were tested with wild type NIH3T3 fibroblasts as well as NIH3T3 cells expressing vinculin-eGFP (kindly provided by K. Miroshnikova and C. Albiges-Rizo, Institute for Advanced Biosciences INSERM U823/ERL CNRS 3148, Grenoble) previously cultured at 37 °C in a humidified 5% $CO_2$ incubator with Dulbecco Modified Essential Medium D-GlutaMAX (Gibco) supplemented with 1% Penicillin Streptomicin (Sigma) and 10% fetal bovine serum (Gibco). The cells were seeded at low density on the magneto-active substrates coated with fibronectin (around $3{\cdot}10^3$ cells/cm$^2$). The magneto-active substrates and the fluorescent cells were imaged on an epifluorescence microscope (Olympus IX83) equipped with a white laser (Fianium) to excite the fluorescent beads and the eGFP.

Cell response was assessed by imaging the eGFP fluorescence and the dark-red fluorescent beads every 4 s, during a 30 min experimental procedure, which consists of a 10 min rest, followed by a 5-minute dynamic stimulation with a 0.25 Hz rectangular signal of 5 A current input in the electromagnets, and a final 15 min rest. The protrusive activity was analysed on 16 cells deformed by the displacement of a magnetic pillar in their close

vicinity and 14 control cells, which were exposed to the same magnetic field but no deformation due to the absence of pillars in their surroundings. In both cases, cells with a sufficient cytosolic eGFP-Vinculin signal were chosen to allow for an automatic tracking of their boundary. Cell culture and experiments were carried out in accordance with the relevant guidelines and regulations.

**Image analysis.** *Cell traction and pillar-induced deformation measurement.* Cell traction force microscopy (TFM)[32] and quantification of the deformation induced by pillar actuation were performed with the same algorithm. Surface displacements were determined from images of the fluorescent beads: in the case of the pillars, the images with and without application of the magnetic field were compared, while in the case of cell traction measurements, the bead images in the presence of cells were compared to the reference image obtained after washing the cells away. After correction for experimental drift, the images were divided into $256 \times 256$ pixel square sub-images ($34 \times 34\,\mu m^2$). First, cross-correlation was used to yield the average displacement on each pair of sub-images, which were shifted accordingly. The fluorescent beads were then tracked with high accuracy (20 nm) to obtain a displacement map with high spatial resolution[33]. The final displacement was obtained on a square grid with 1 µm spacing using linear interpolation. Force reconstruction was carried out under the assumption that the substrate is a linear elastic half space considering in-plane stress only, using Fourier Transform Traction Cytometry with zeroth-order regularization[34]. The problem of calculating the stress field ($T_x$ and $T_y$) from the displacement was solved in Fourier space, then inverted back to real space. The final stress magnitude $\sqrt{T_x^2 + T_y^2}$ was obtained on a grid with 1 µm spacing. To distinguish clearly the regions undergoing traction and those under compression, the derivative of the stress was calculated with respect to each direction using the central difference method, and the sign of $\frac{dT_x}{dx} + \frac{dT_y}{dy}$ gives the type of stress applied on the PDMS surface. Positive stress variations correspond to tensile stress whereas negative ones correspond to compressive stress.

To monitor the effect of a sequence of actuation on cell traction, images of fluorescent beads were recorded every 4 seconds for 30 min starting with 10 min of rest, followed by 5 min of mechanical stimulation, after which the cells were again at rest for 15 min. Finally the cells were washed away with 0.2% SDS to capture the reference bead image without any magnetic field. The traction stress map was calculated for each frame. The strain energy, which is the mechanical energy transferred from the cell to the substrate, was calculated as

$$E = \frac{1}{2}\int_{cell} \mathbf{T}(\mathbf{r}).\ \mathbf{u}(\mathbf{r})\ d^2\mathbf{r}$$

where $\mathbf{T}(\mathbf{r})$ is the stress vector and $\mathbf{u}(\mathbf{r})$ the displacement vector. To highlight the change in traction spatial distribution, we subtracted the traction map averaged over 100 frames after stimulation (corresponding to a time period of 6′40″), from the stress map averaged over the same period immediately before stimulation. This difference map shows positive areas corresponding to traction reinforcement and negative ones corresponding to traction relaxation. All calculations and image processing were performed with Matlab R2015b and figure generation was done with Python.

*Protrusion activity of the cells.* eGFP-Vinculin Images were first Gaussian filtered to reduce noise and thresholded to obtain a mask of the cell. The contour velocity was evaluated using a previously described method[35,36]. The normal velocity v(x,y,t) was estimated as

$$v(x, y, t) = \frac{[I(x, y, t + \Delta t) - I_0] - [I(x, y, t - \Delta t) - I_0]}{|\nabla I(x, y, t)|}$$

where $I(x, y, t)$ is the grey level at position $(x, y)$ and time t, $I_0$ is the same threshold as the one used to obtain the masks, $|\nabla I(x, y, t)|$ is the local gradient magnitude, and $\Delta t$ is a number of frames (here 10 frames i.e., 40 s).

For each cell, a velocity map was derived by (i) averaging velocity values of each boundary pixel of the cell and its 12 nearest neighbours and (ii) sorting these resulting values as a function of the normalized position along the perimeter of the cell at a given time. The color-coded smoothed velocities along the normalized perimeter were then displayed as a function of time throughout the experiment. To obtain a unique value for each cell, we extracted and averaged the 5% highest velocity values for each frame (see Supplementary Fig. S8). The ratio between the average maximum velocity of a 5-minute period after and that of the 5-minute period before mechanical stimulation was then calculated.

**Data availability.** The datasets generated and/or analyzed during the current study are available from the corresponding authors on reasonable request.

## Results and Discussion

Magneto-active substrates were fabricated by incorporation and organization of magnetic micro-pillars in a continuous layer of soft elastomer (Fig. 1). The elements involved in the fabrication and actuation of the magneto-active substrates were characterized, before plating cells on their surface and measuring their protrusive activity after stimulation, to demonstrate the potential of this technology for mechanobiology studies.

**Physical properties of the pillars.** Since the aim is to produce a torque on the soft magnetic element embedded in the elastomer, the element needs to be anisotropic in shape (if it were magnetically soft but isotropic in shape, the magnetic moments would simply rotate to align with the applied field, resulting in no tilting of the object itself). The considered micro-pillars consist of a core shell structure, based on a silicon cylindrical

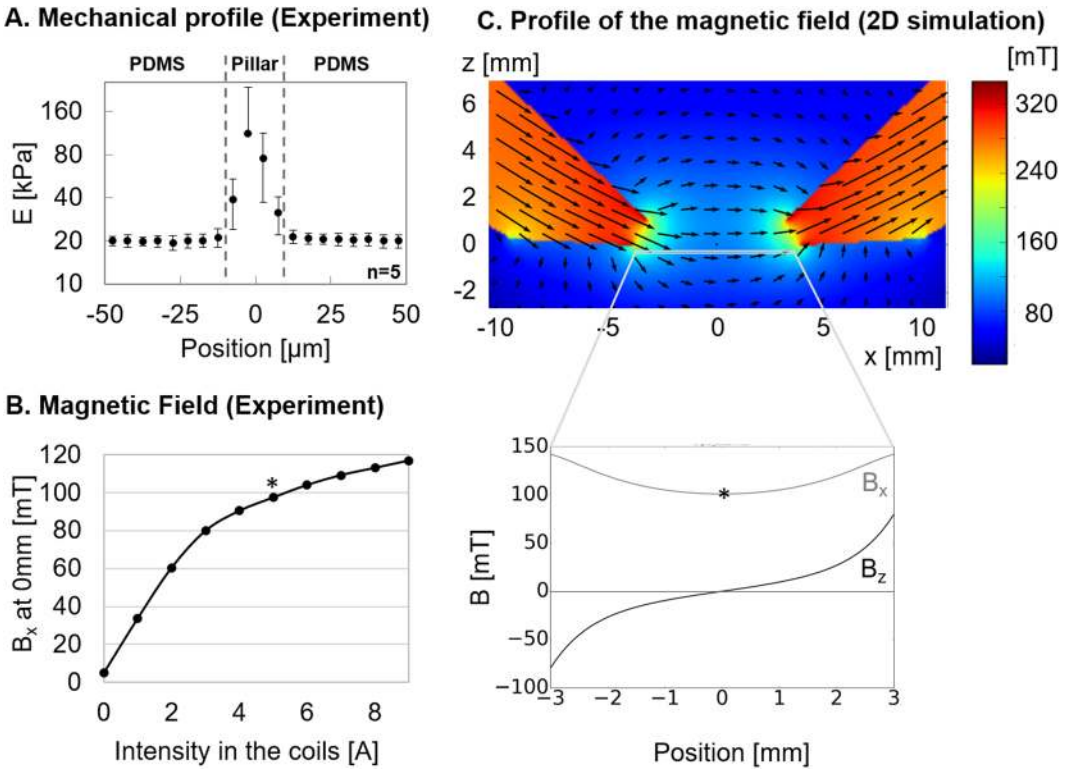


**Figure 2.** Characterization. (**A**) Mechanical profiles of the magneto-active substrate measured around 5 pillars by atomic force microscopy reveal homogeneous PDMS substrates with local increases of the Young modulus above the pillars. (**B**) The horizontal component of the magnetic field $B_x$ increases with the current input to the electromagnets and reaches 100mT for 5 A (*) at the mid-position between the two pole pieces. (**C**) A numerical model in 2D evaluates the distribution of the horizontal and vertical components of the magnetic field ($B_x$ and $B_z$ respectively) between the bevel shaped pole pieces of the electromagnets.

core coated with an iron shell, produced by lithography, DRIE and Fe deposition (Fig. 1A). After collection, the dimensions of 39 pillars were measured to be $33.5 \pm 2.5$ µm in height and $15.7 \pm 1.2$ µm large. This indicates that the micro-pillars are broken roughly 10 µm above their base, which corresponds to the thickness of Fe deposited between the pillars. The saturation magnetic moment of about $8{\cdot}10^4$ pillars was estimated to be $3.3{\cdot}10^{-2}$ A.m$^2$, i.e., $4.1{\cdot}10^{-9}$ A.m$^2$ per pillar. Considering that the saturation magnetization of iron is $1.7{\cdot}10^6$ A.m$^{-1}$, the volume of iron deposited on a given pillar is estimated to be around 2400 µm$^3$, which matches the order of magnitude obtained from a geometrical estimation.

The protocol of assembly established in the methods section produces magneto-active substrates containing magnetic micro pillars arranged in a layer of soft PDMS according to the chosen magnetic template (see Fig. 1B). To better control the position of the pillars, we tried using template arrays of magnetic islands that could trap individual magnetic micro-pillars at regular distances. However, trapping one pillar per island proved difficult. It is important to mention that organizing the pillars using a stripe-template does not affect their ability to locally deform the substrate, provided that the pillar density is kept low enough to prevent magnetic and mechanical interactions between pillars.

**Mechanical properties of the substrate.** PDMS is a biocompatible elastomer widely used as a cell substrate. We first observed that standard Sylgard 184 used in a ratio base to crosslinker of 40:1, leads to a substrate with a Young's modulus of 40kPa and a sticky surface. We found that adding 8 parts of silicone oil to the Sylgard mixture reduced both the rigidity, to a suitable range to be deformed by cells so as to probe their contractile forces, and the stickiness of the surface, to facilitate handling of the samples. The mechanical properties measured on 3 samples of soft PDMS with a rheometer indicate that both the shear storage modulus G′ and the shear loss modulus G″ are independent of the amplitude of deformation $\gamma$ between 0.01% and 20% of shear when deformed at 1 Hz (see Supplementary Fig. S1), with $G' = 6756$ Pa and $G'' = 1117$ Pa. However, varying the frequency between 0.01 Hz and 10 Hz of a 10% shear reveals that below 0.2 Hz, G″ becomes an order of magnitude inferior to G′ which is about 6000 Pa. The material's behaviour is thus dominated by elasticity as indicated by the phase angle $\delta = Arc\ tan\left(\frac{G''}{G'}\right)$, which remains close to 0 at the frequencies of interest (see Supplementary Fig. S1). For homogeneous isotropic linear elastic materials, Young's modulus can be derived as $E = 2{\cdot}(1+\nu){\cdot}G'$. Since Poisson's modulus of our PDMS is $\nu = 0.418$[37], we estimate E = 19.2kPa when deformed at 1 Hz. This global value matches the results of 5 mechanical profiles obtained by atomic force microscopy, as the local Young's modulus obtained away from a pillar is $E = 20.3 \pm 2$ kPa (Fig. 2A). The PDMS mixture used in this study leads to a soft

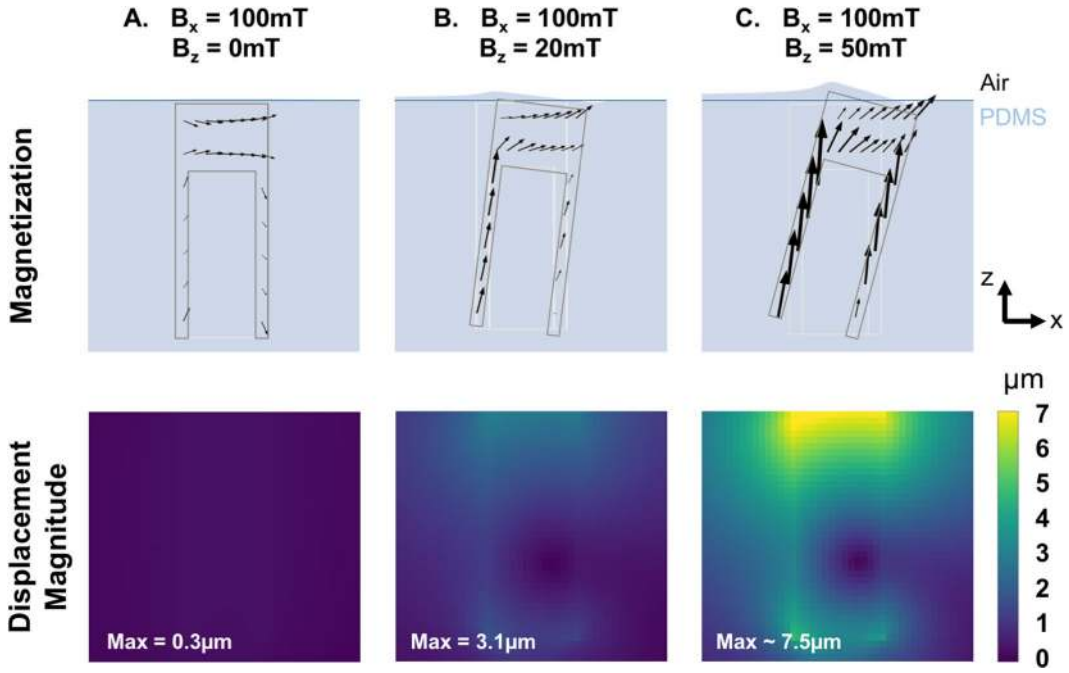


**Figure 3.** Contribution of $B_z$. The magnetization of the iron pillar induced by a purely horizontal magnetic field (**A**), a magnetic field with a slight (**B**) or large (**C**) vertical component $B_z$ and the subsequent magnitude of displacement in the substrate have been predicted with the magneto-mechanical model. In each case, the undeformed positions of the PDMS free surface and the pillar are represented by blue and light grey lines, respectively.

substrate with negligible viscosity at the frequencies of interest, and thereby allows us to use the TFM algorithm and derive force field from the displacement field of the fluorescent beads.

As expected, the rigidity sharply increases by an order of magnitude when indenting above the pillars (Fig. 2A), which leads us to avoid analysing cells lying above pillars.

The layer of soft PDMS is $115.5 \pm 12.5$ μm thick, as measured in 9 points of 3 different samples. As shown in Fig. 1B, this layer is thick enough to neglect the effect of the glass coverslip on the mechanical properties of the substrate and on the pillar displacement close to the surface, while thin enough to have optical properties compatible with fluorescence imaging. Of note, the fluorescent beads embedded under the surface of the soft PDMS are homogeneously dispersed in a single plane with an average density of 0.2 beads/μm², including above the pillars, as verified from images taken on a substrate positioned upside-down (see Supplementary Fig. S2). This density of beads is low enough to neglect their influence on the mechanical behaviour of the soft substrate[38,39] and allows automated tracking of the displacement with high accuracy (20 nm) and spatial resolution (<5 μm). This reproducible method of bead incorporation is thus particularly suited to improve TFM on a soft elastomer[40] and widens the range of soft substrates that can be used to study cell contractility.

**Generation of the magnetic field.** To actuate the magnetic micro-pillars, two electromagnets have been designed to generate a predominantly in-plane magnetic field (Fig. 1C). While the iron pole pieces have been designed to focus the field at the surface of the magneto-active substrate, the dimensions and the position of the electromagnets were determined by the geometrical constraints related to the microscope and the cell culture dishes.

The $B_x$ component of this field was measured as a function of current input into the coils with a Hall probe positioned at the mid-point between the two pole pieces (Fig. 2B). We restricted the current input to a maximum intensity of 5 A for the rest of the experiments, which corresponds to a magnetic field of 100 mT.

The magnetic field distribution calculated within the actuation zone is represented in Fig. 2C. This simulation indicates that the $B_x$ component of the magnetic field is relatively homogeneous in-between the electromagnets, while the vertical component ($B_z$) varies symmetrically with respect to the centre, where it vanishes. In the plane of the pillars and roughly 70 μm below the electromagnets, if $B_x$ is set to ~100mT in the middle, as generated with 5 A in the coils, then $B_z$ varies from 0mT (exactly mid-way between the electromagnets) to ±70mT (near the poles' apex). The important role of the out-of-plane component is discussed below.

**Actuation of the substrate.** *Influence of $B_z$.* The $B_z$ component of the applied field serves to induce a vertical component of the magnetization of the micro-pillars. This in turn allows the $B_x$ component of the applied field to produce a torque on the micro-pillars. The role of $B_z$ in inducing a mechanical response of the substrate was assessed within the framework of the magneto-mechanical model, by varying $B_z$ between 0 and 70mT while fixing the horizontal field $B_x$ at 100mT and neglecting the $B_y$ component. Figure 3A shows the vertical cut of a

pillar experiencing a purely horizontal magnetic field ($B_z = 0$). The magnetization of the pillar lies practically in the horizontal plane and there is no significant torque on the pillar. However, as soon as the pillar experiences a vertical field component $B_z$, even small compared to $B_x$, the magnetization in the sidewalls tends to align along the long axis, forming a non-zero angle with the applied field, and resulting in an effective torque on the pillar. Pillars experiencing a vertical magnetic field of 20mT are predicted to produce displacements of around 3.1 µm at the surface of the PDMS (Fig. 3B). These simulations show that a non-zero vertical component of the magnetic field $B_z$ is essential to take advantage of the shape anisotropy of the iron shell to align the magnetization of the pillar along its long axis, and thereby generate a torque able to deform the surface of the substrate. Figure 3C indicates that this effect is modulated by the value of the vertical magnetic field, since for $B_x = 100$mT and $B_z = 50$mT, the surface above the pillar is expected to experience in-plane displacements of over 7.5 µm. Note that the slight vertical distortion (<1 µm) expected close to the tilted pillar at high deformation was observed experimentally through a local defocusing of the fluorescent beads.

The magneto-mechanical model indicates that the displacement generated by a pillar decreases with increasing distance from the closest pole piece, which was observed experimentally (see Supplementary Fig. S3). Thus in a given experiment with cells spread across the substrate, the influence of different values of displacement on a given set of cells can be studied.

*Experimental deformation.* The magneto-mechanical simulation of a pillar placed at 1 mm from a pole piece was performed with $B_x = 119$mT and $B_z = 27$mT, as estimated from the magnetic field distribution simulation of the experimental actuation system (Fig. 2C). A top view of the displacement field in the *xy* plane was used to estimate the stress magnitude of the surface using the traction force microscopy algorithm, and the stress variations. These numerical estimations agree with experimental measurements performed on 5 pillars significantly actuated by electromagnets powered with 5 A ($B_x \sim 100$mT, $B_z \sim 70$mT). Indeed, such actuation generates a displacement field that decays sharply by 50% within 20 µm (Fig. 4A), which corresponds to the cellular length scale. The resulting deformation of the surface is qualitatively symmetric with respect to the pillar.

The displacements induced by a series of 15 pillars aligned about 1.5 mm away from the pole piece tip ($B_z \sim 20$mT) and experiencing an incremental actuation (from 0 to 5 A in the coils) was systematically measured to estimate the variability of the actuation between pillars (see Supplementary Fig. S4). The broad distribution of maximum displacements, which increases with the current input, can be explained by the influence of pillar geometry on the resulting actuation. 3D magneto-mechanical simulation was performed on core-shell pillars with different shapes (cylinder and cone of different heights), and positioned with the iron cap either towards the surface (up) or towards the coverslip (down) (see Supplementary Fig. S5). We found that cylinders are insensitive to the up/down orientation whereas conical pillars are sensitive to it, showing a 50% displacement increase when placed upside down. Hence, a conical pillar with iron cap up induces 25% less deformation than a cylindrical one, but when placed upside down the obtained deformation becomes larger than that of a cylindrical pillar. Regarding the influence of the pillar length, which can be affected during mechanical collection from the wafer, we found that a cylindrical pillar is expected to deform the surface about 22% less if reduced by 5 µm from its base, and up to 45% less if reduced by 10 µm.

Coupling the active substrates with TFM allows to measure the actual displacements and stresses induced by each pillar after removal of the cells. Hence, the variability of actuation amplitudes from pillar to pillar can be used to our advantage: a range of stimuli can be explored in one experiment, where the precise stress applied on each cell is known.

Deriving the stress magnitudes at the surface of the 20kPa PDMS reveals that the magneto-active substrates allow generating a stress within 30 µm around the pillars, up to 2.4kPa of stress amplitude in the close vicinity of the pillars (Fig. 4B). Such a value corresponds to the range of stress that cells are able to generate on their substrate[41,42] and therefore supports the relevance of the present system in mimicking the mechanical coupling of neighbouring cells through their matrix[43]. In terms of force, magneto-active substrates can locally transmit nN-forces to cell adhesions, if a typical adhesion surface of 1µm$^2$ is considered, which also compares to forces generated by single adhesions[44,45]. Moreover, the maps of stress variation show a clear localization of the mechanical stimulation in a 30µm-radius around the pillars. This subcellular length scale confirms that the present magneto-active substrates are appropriate tools to investigate the spatiotemporal evolution of intracellular signals triggered by a local extracellular mechanical cue sensed at the focal adhesions.

Displaying the stress variation map also highlights the different modes of stimulation available with the magneto-active substrates. Indeed, the torque applied by the magnetic field on a pillar stresses the surface in tension on one side (positive stress variation) and in compression on the other side (negative stress variation). This feature offers the possibility to perform both stretching and compression experiments on the same setup and thus to propose rigorous comparisons of the differential response of stimulated cells. This is particularly relevant to investigate muscle cells, cell types sitting in weight bearing tissues[25,46] but also stem cells, the differentiation of which is already known to be tuned by static mechanical cues of their environment such as stiffness[12] and geometry[5] via mechanotransduction processes.

*Control through the current input.* Electromagnets rather than permanent magnets were chosen to facilitate dynamic control of the system. As expected from the evolution of the magnetic field measured experimentally (Fig. 2B), the deformation, stress and stress variation profiles progressively spread along the x direction up to 5 A and stabilize thereafter (see Supplementary Fig. S6). This observation supports our choice to limit the stimulations to 5 A for subsequent experiments. Cyclic stimulations manually performed between 0 and 5 A on 4 different pillars show that the temporal pattern of deformation is reproducible over several cycles of actuation (Fig. 4D). The residual deformation appearing after the first cycle can be explained by a slight defocusing of the surface around

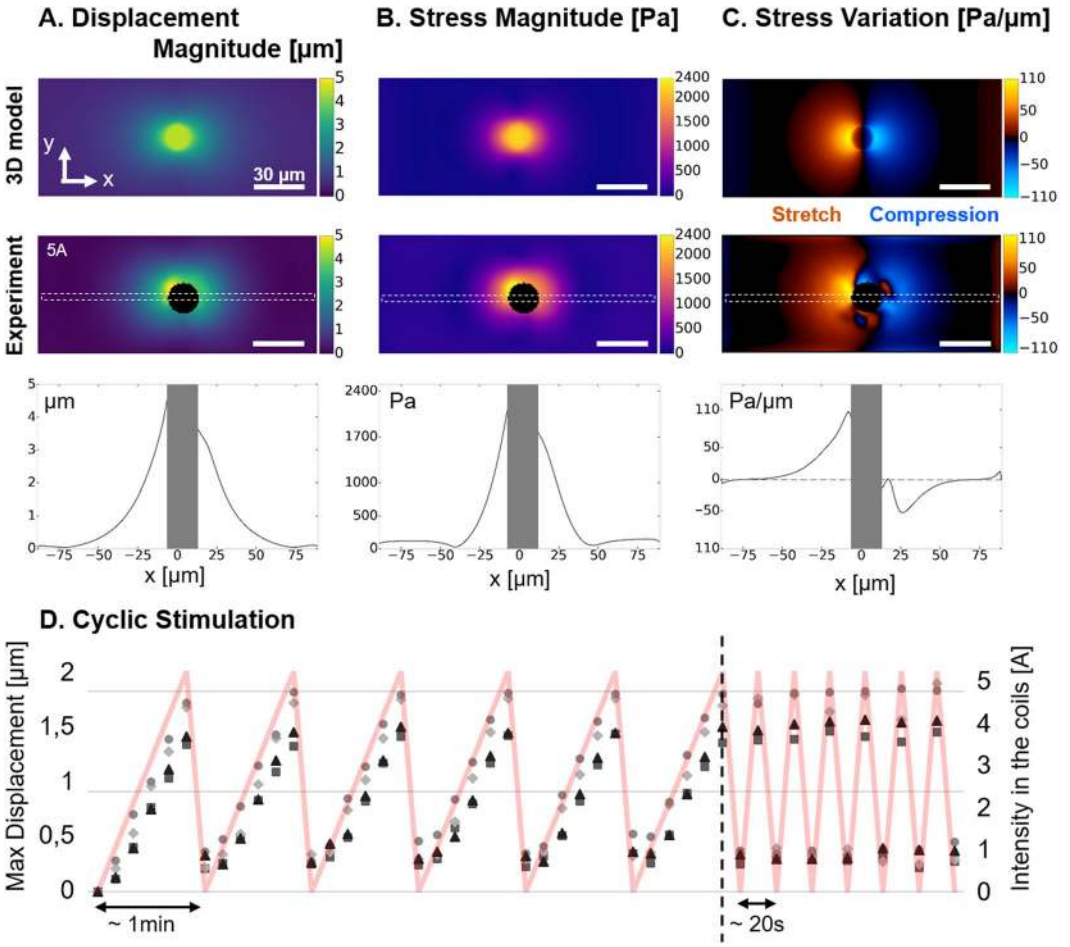


**Figure 4.** Actuation of the substrate. (**A**) The magnitude of displacement induced by a pillar positioned 1 mm away from the electromagnet and experiencing $B_x = 119$mT and $B_z = 27$mT was estimated with a 3D model and compared to the magnitude of displacement measured experimentally around 5 pillars stimulated by an electromagnet supplied with 5 A. (**B**) Maps of stress magnitude were derived from the displacement fields by Fourier Transform Traction Cytometry, and (**C**) maps of stress variation were calculated to distinguish the regions under traction and compression. Scale bar: 30 µm. Profiles corresponding to the dashed region of each map are also displayed. (**D**) Maximum magnitude of displacement measured on 4 different pillars undergoing cyclic stimulations applied by manually adjusting the intensity of the current input (red curve).

the pillar and/or a local micro-delamination at the interface between the soft PDMS and the pillar. Besides tuning the stress applied to the cell in a physiological range by varying the amplitude of the current, it is also possible to tune the temporal pattern of the stimulation with a function generator. Micrometric displacements of the pillars were detectable up to 10 Hz with our optical setup, which is comparable to current cell stretcher technologies[8].

**Application to cells.** To test our system in relevant conditions for biological studies, a low density of NIH3T3 fibroblasts was plated on the magneto-active substrates after functionalization of the surface by adsorption of fibronectin. The cells adhered normally and homogeneously within 3 to 4 hours after seeding (Fig. 5A).

First, we investigated whether the stresses induced by a pillar in the vicinity of a cell can mimic the action of neighbouring cells, both in magnitude and spatial patterns. Figure 5B shows that a pillar positioned ~1.5 mm away from the tip of an electromagnet pole piece powered by 5 A, generates up to 1.5kPa stress in the absence of a neighbouring cell, and that NIH3T3 cells also generate up to 1.5kPa when lying close to the same pillar at rest. These values indicate that the forces imposed by the actuation of the magnetic pillar are comparable to the traction forces generated by the cells on the same substrate, which supports the relevance of the method. Furthermore, mapping the stress variations (Fig. 5C) both confirms the symmetric pattern of stretching and compression generated by the pillar and recalls that cells compress the surface they adhere on. Stress variations induced by the actuation of a pillar also appear very similar to those produced by a neighbouring cell, with the juxtaposition of regions that are highly compressed (blue) and regions that are highly stretched (yellow).

We show that the magneto-active substrates are fully compatible with fluorescence imaging techniques (Fig. 6A). As such, the precise location of a cell with respect to a pillar is obtained by combining the fluorescence images of dark red fluorescent beads with those of fibroblasts expressing eGFP vinculin. Supplementary Fig. S7

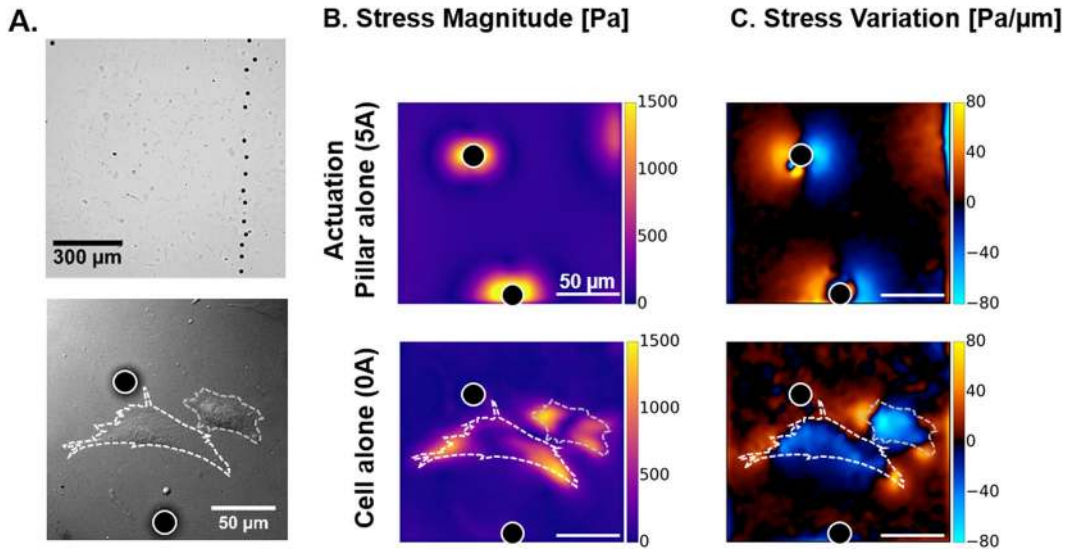


**Figure 5.** Cells on magneto-active substrates. (**A**) Bright field images of NIH3T3 fibroblast cells spread on a magneto-active substrate. Stress magnitude (**B**) and variation (**C**) experienced by the surface were measured under the action of a pillar without cell (5 A) and in the presence of contractile cells in the vicinity of a pillar at rest. Scale bar: 50 µm.

and Movie S9 reveal that increasing gradually the current in the electromagnets not only deforms the surface but also the adhering cell, and thus demonstrate the possibility to tune the amplitude of mechanical stimulation induced by the active substrate.

Then, we performed live-cell experiments and investigated the cellular response to a 5-minute dynamic stimulation at 0.25 Hz. Figure 6A shows the fluorescent image of a NIH3T3 fibroblast expressing Vinculin-eGFP (green) overlaid with the fluorescent signal from the beads used for TFM (red). Upon actuation of the magnetic pillar nearby (white circle), the cell was deformed with a local maximal displacement of 3.8 µm as illustrated by the different cell contours drawn in Fig. 6A (yellow outline). Shortly after the end of the stimulation period, a new protrusion appeared on the opposite side (Fig. 6A, magenta outline, Supplementary Movie S10). To quantify the overall increase of protrusive activity observed on several cells, we estimated the normal velocity of the cell boundaries using a method introduced by Döbereiner *et al.*[35]. Velocity profiles along the normalized perimeter of the cell were represented as a function of time as in a kymograph (Fig. 6B). In this example, the cell rapidly develops and retracts a protrusion with velocities of +5 µm/min and −5 µm/min, respectively, as shown by the red and blue streaks. The same protocol of mechanical stimulation and data analysis was applied to 16 different cells, and 14 control cells experiencing the same magnetic field but no mechanical stimulation. We compared the velocity of the most active border region before and after the mechanical stimulation (see Methods and Supplementary Fig. S8). The velocity ratios shown in Fig. 6B show different distributions between the control and the stimulated populations ($p < 0.05$, Mann-Whitney rank test). The response is nevertheless not clear as half of the cells increased significantly their protrusive activity after dynamic mechanical stimulation, while the rest of the population is comparable to the control cells. This observation is consistent with the results of Nagayama *et al.* where, after stimulating cells with discrete pillars, they observed two categories of responses, both in force and in cell area[21].

To prove the inherent compatibility of our setup with time-resolved TFM, we show the mechanical response of an exemplary cell in Fig. 6C (see also Supplementary Movies 10). This cell showed a well-defined force dipole before the actuation (Fig. 6C 0 A) which was strongly perturbed when the pillar was displaced (Figs 5A and 6C). The traction maps were calculated for every frame of the movie and three regions of interest (ROI) were chosen to display the dynamic mechanical response. The first ROI, close to the pillar, showed the periodic stimulation corresponding to the pillar actuation and a fast and maintained reinforcement from about 400 Pa up to 650 Pa (see Fig. 6C, Supplementary Movies 10). In contrast, the second ROI, chosen on the other side of the cell, displayed a strong relaxation from about 500 Pa down to 300 Pa starting also from the very beginning of the stimulation. The third ROI was chosen at a place of high pre-tension and, although placed about 50 µm away from the pillar, the average stress in this ROI also showed an immediate response (see Supplementary Movies 10) and a sustained reinforcement (from 1400 Pa to 1500 Pa). We can speculate that the immediate mechanical response is the result of a direct mechanical transmission at a distance through the cytoskeleton and adhesion crosslinks[47]. Overall, this cell showed no dramatic change in its strain energy, except during the mechanical stimulation where the periodic stress due to the pillar displacement was clearly visible. The strain energy being stable shows that this cell did not increase or decrease its contractility but rather redistributed the forces. To get a global view of the cell mechanical response, we compared the average stress maps obtained during about 6 minutes before and 6 minutes after the stimulation. The resulting traction difference map (Fig. 6C) reveals a heterogeneous response within the cell with alternating reinforcement and relaxed areas. Even if both relaxation and reinforcement seem more intense in the part of the cell directly displaced by the pillar, the traction difference map shows that this local

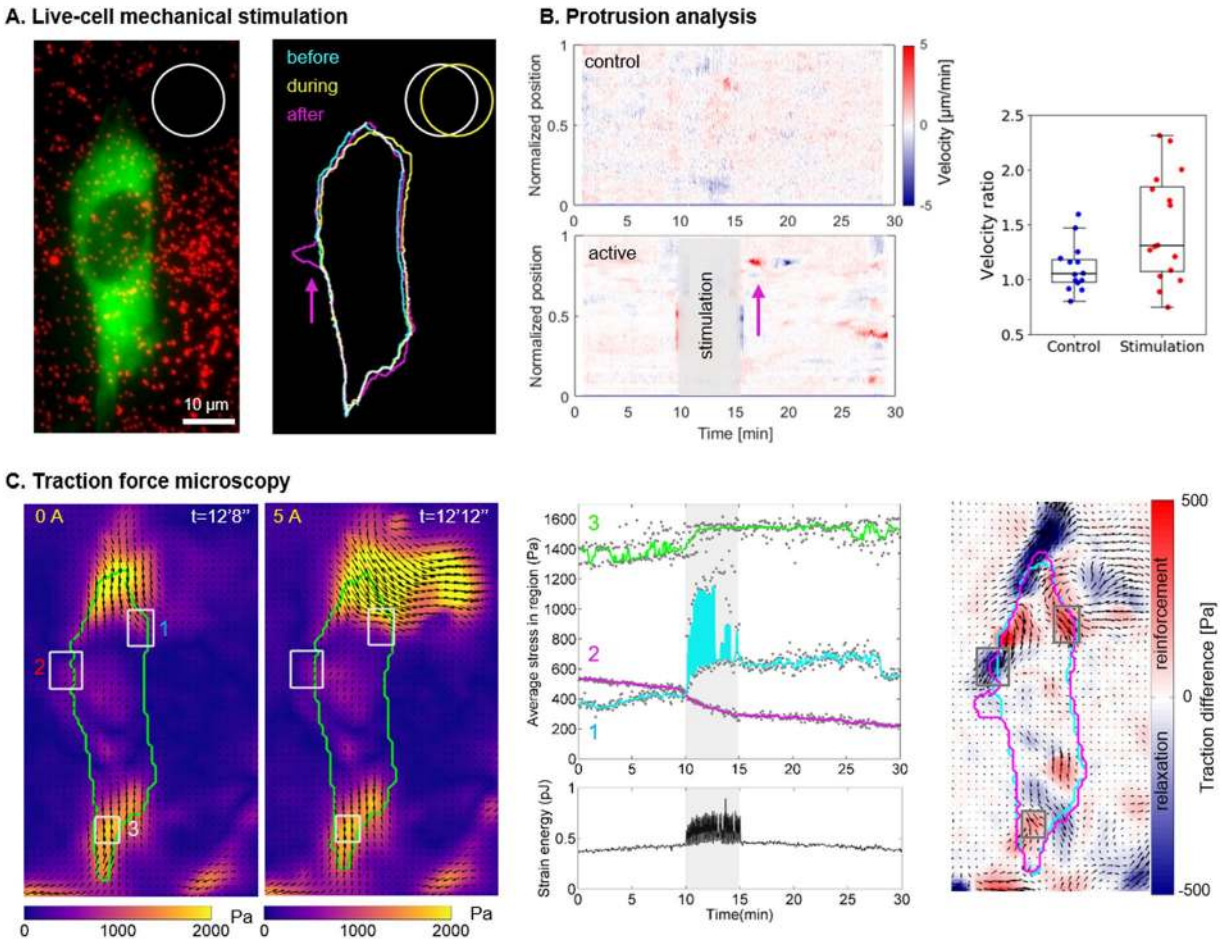


**Figure 6.** Cell response to stimulation. (**A**) Fluorescent images of a NIH3T3 vinculin-eGFP fibroblast (green) and the beads spread under the surface (red) were used to draw the contours of the cell and the pillar, respectively. The cell was deformed (yellow) when the pillar was displaced, and a new protrusion appeared (magenta) a few minutes later. Corresponding movie as supplementary material (Movies 10) (**B**) Protrusion analysis. Velocity profiles of the boundary of a control cell and the stimulated cell (**A**) along a normalized perimeter as a function of time. Positive values (red) represent protrusions whereas negative values (blue) represent retractions. On the stimulated cell, a protrusion is visible (magenta arrow) shortly after the end of the stimulation and followed by a retraction. Quantification of the cellular response for 16 stimulated cells and 14 control cells: ratio of velocity after and before the stimulation were calculated as detailed in Fig. S8 and plotted for each cell. Approximately half of the cell population showed an increased protrusion activity after the mechanical stimulation. (**C**) Stress maps of the cell and the pillar at rest (0 A) and during actuation (5 A). Such maps were derived every 4 s during the entire protocol and the average stress in the 3 regions of interest (grey rectangles) and the strain energy of the cell (green contour) were plotted as a function of time. Map representing the local differences in averaged traction values before and after 5 min stimulations: blue indicates a local relaxation of the cell, and red indicates a reinforcement of the traction forces. The corresponding movie is given in the supplementary materials (Movies 10).

mechanical stimulation induced a global reorganization of the cell tensions. Nevertheless, the TFM analysis of 10 stimulated cells did not reveal any clear trend on a cellular mechanical reaction to the dynamic deformation (see Supplementary Fig. S11) as also observed by Sniadecki *et al.*[19] and Nagayama *et al.*[21]. The random positioning of the cells with respect to the magnetic pillars constitutes a current limitation of the system as it leads to different types of stimulation for each cell. Taken together with the heterogeneity of the mechanical response at the single cell scale, it makes it difficult and out of the scope of this paper to identify relevant readouts of a reproducible cellular mechanical response. This relative positioning of cells with respect to the pillars may explain as well the diversity in the protrusive activity response (Fig. 6B). Because a polarized cell may react differently if pulled at the front or at the back[48], or along different orientations, patterning adhesive islands on the substrate appears to be a relevant solution to normalize the experiments by normalizing cell shape and position with respect to the pillars. Other magnetically actuated systems proposed previously were designed to stimulate cells with discrete surfaces either at a subcellular scale[19,21] or in large cell migration chips[49]. The present method addresses length scales from subcellular to cellular levels, with displacements spanning continuously over larger distances (see Fig. 5B). A specificity of the magneto-active substrates is to provide a continuous adhesive surface thereby not restricting

the adhesion dynamics and distribution and allowing the cells to freely respond to the stimulation. As such, force dynamics and distribution can be quantified continuously using traction force microscopy.

## Conclusion and Outlook

The magneto-active substrates developed here complement the current cell stretching technologies used to establish that cells change contractility, spreading phenotype, fibre formation and proliferation differently for different mechanical stimulation patterns[8,17–19]. Indeed, the present work demonstrates that magneto-active substrates made of soft magnetic micro-pillars embedded in a soft elastomer uniquely combine advantages that were not associated so far. The magneto-active substrates (i) have been designed to meet criteria relative to biocompatible materials and optical compatibility with high-resolution fluorescence microscopy, (ii) enable to apply a local and controlled mechanical stimulation on single cells spread on a continuous surface, and (iii) have an additional potential to quantify cellular mechanical responses via time-resolved traction force microscopy. Live-cell experiments including a period of dynamic deformation via the magneto-active substrates further support the relevance of this new tool in the study of cell response to mechanical stimulation.

Alternative approaches to micro-pillar fabrication (e.g. electro-deposition in patterned moulds) and template preparation (e.g. electro-deposition in patterned moulds or chemical etching of foils) can be explored to improve the reproducibility of actuation from pillar to pillar. The use of hard magnetic micro-pillars, which would be permanently magnetized in a given direction, could also be studied.

Patterning adhesive islands on the surface, as done in[32,50], would overcome the limitations related to the positioning and orientation of the cells with respect to the pillars. A strategic functionalization of the magneto-active substrate would then guarantee the repeatability of cell experiments by controlling the degree of spreading and the geometry of the cell. Most importantly, patterning would enable to choose the mode of stimulation (stretching, compression or shear) and the distance to the pillar. This improvement would also constitute a first step towards high throughput experiments. In the long term, we believe that magneto-active substrates have potential to become a standard tool to investigate single cell or multicellular response to dynamic mechanical stimulation and thus improve our quantitative understanding of mechanotransduction.

## References


1. Jaalouk, D. E. & Lammerding, J. Mechanotransduction gone awry. *Nat. Rev. Mol. Cell Biol.* **10**, 63–73 (2009).
2. Chin, L., Xia, Y., Discher, D. E. & Janmey, P. A. Mechanotransduction in cancer. *Curr. Opin. Chem. Eng.* **11**, 77–84 (2016).
3. Lo, C. M., Wang, H. B., Dembo, M. & Wang, Y. L. Cell movement is guided by the rigidity of the substrate. *Biophys. J.* **79**, 144–152 (2000).
4. Engler, A. J. *et al*. Matrix elasticity directs stem cell lineage specification. *Cell* **126**, 677–89 (2006).
5. Ruiz, S. A. & Chen, C. S. Emergence of Patterned Stem Cell Differentiation Within Multicellular Structures. *Stem Cells* **26**, 2921–2927 (2008).
6. Riveline, D. *et al*. Focal contacts as mechanosensors: externally applied local mechanical force induces growth of focal contacts by an mDia1-dependent and ROCK-independent mechanism. *J. Cell Biol.* **153**, 1175–1186 (2001).
7. Grashoff, C. *et al*. Measuring mechanical tension across vinculin reveals regulation of focal adhesion dynamics. *Nature* **466**, 263–6 (2010).
8. Cui, Y. *et al*. Cyclic stretching of soft substrates induces spreading and growth. *Nat. Commun.* **6**, 6333 (2015).
9. Jungbauer, S., Gao, H., Spatz, J. P. & Kemkemer, R. Two characteristic regimes in frequency-dependent dynamic reorientation of fibroblasts on cyclically stretched substrates. *Biophys. J.* **95**, 3470–3478 (2008).
10. Livne, A., Bouchbinder, E. & Geiger, B. Cell reorientation under cyclic stretching. *Nat. Commun.* **5**, 3938 (2014).
11. Sears, C. & Kaunas, R. The many ways adherent cells respond to applied stretch. *J. Biomech.* **49**, 1347–1354 (2016).
12. Sweeney, H. L., Discher, Engler, A. J. & S. Matrix elasticity directs stem cell lineage specification. *Cell* (2006).
13. Kim, D.-H., Wong, P. K., Park, J., Levchenko, A. & Sun, Y. Microengineered platforms for cell mechanobiology. *Annu. Rev. Biomed. Eng.* **11**, 203–233 (2009).
14. Haase, K. & Pelling, A. E. Investigating cell mechanics with atomic force microscopy. *J. R. Soc. Interface* **12**, 20140970 (2015).
15. Wang, N., Butler, J. P. & Ingber, D. E. Mechanotransduction across the cell surface and through the cytoskeleton. *Science* **260**, 1124–1127 (1993).
16. Hénon, S., Lenormand, G., Richert, A. & Gallet, F. A new determination of the shear modulus of the human erythrocyte membrane using optical tweezers. *Biophys. J.* **76**, 1145–51 (1999).
17. Quinlan, A. M. T., Sierad, L. N., Capulli, A. K., Firstenberg, L. E. & Kristen, L. Combining Dynamic Stretch and Tunable Stiffness to Probe Cell Mechanobiology *In Vitro*. **6** (2011).
18. Krishnan, R. *et al*. Reinforcement versus fluidization in cytoskeletal mechanoresponsiveness. *PLoS One* **4**, e5486 (2009).
19. Sniadecki, N. J. *et al*. Magnetic microposts as an approach to apply forces to living cells. *Proc. Natl. Acad. Sci. USA* **104**, 14553–8 (2007).
20. Digabel, J. *et al*. Magnetic micropillars as a tool to govern substrate deformations. *Lab Chip* **11**, 2630 (2011).
21. Nagayama, K., Inoue, T., Hamada, Y. & Matsumoto, T. A novel patterned magnetic micropillar array substrate for analysis of cellular mechanical responses. *J. Biomech.* **65**, 194–202 (2017).
22. Cavalcanti-Adam, E. A. *et al*. Cell spreading and focal adhesion dynamics are regulated by spacing of integrin ligands. *Biophys. J.* **92**, 2964–74 (2007).
23. Frey, M. T., Tsai, I. Y., Russell, T. P., Hanks, S. K. & Wang, Y.-L. Cellular responses to substrate topography: role of myosin II and focal adhesion kinase. *Biophys. J.* **90**, 3774–3782 (2006).
24. Roberts, S. R., Knight, M. M. & Lee, D. a & Bader, D. L. Mechanical compression influences intracellular Ca2+ signaling in chondrocytes seeded in agarose constructs. *J. Appl. Physiol.* **90**, 1385–1391 (2001).
25. Szafranski, J. D. *et al*. Chondrocyte mechanotransduction: Effects of compression on deformation of intracellular organelles and relevance to cellular biosynthesis. *Osteoarthr. Cartil.* **12**, 937–946 (2004).
26. Desprat, N., Supatto, W., Pouille, P.-A., Beaurepaire, E. & Farge, E. Tissue deformation modulates twist expression to determine anterior midgut differentiation in Drosophila embryos. *Dev. Cell* **15**, 470–7 (2008).
27. Cheng, G., Tse, J., Jain, R. K. & Munn, L. L. Micro-Environmental Mechanical Stress Controls Tumor Spheroid Size and Morphology by Suppressing Proliferation and Inducing Apoptosis in Cancer Cells. *PLoS One* **4**, e4632 (2009).
28. Montel, F. *et al*. Stress clamp experiments on multicellular tumor spheroids. *Phys. Rev. Lett.* **107**, 1–4 (2011).
29. Tse, J. M. *et al*. Mechanical compression drives cancer cells toward invasive phenotype. *Proc Natl Acad Sci USA* **109**, 911–916 (2012).
30. Kustov, M. *et al*. Magnetic characterization of micropatterned Nd–Fe–B hard magnetic films using scanning Hall probe microscopy. *J. Appl. Phys.* **108**, 63914 (2010).

31. Dempsey, N. M. *et al*. Micro-magnetic imprinting of high field gradient magnetic flux sources. *Appl. Phys. Lett.* **104**, 262401 (2014).
32. Tseng, Q. *et al*. A new micropatterning method of soft substrates reveals that different tumorigenic signals can promote or reduce cell contraction levels. *Lab Chip* **11**, 2231–2240 (2011).
33. Crocker, J. & Grier, D. Methods of Digital Video Microscopy for Colloidal Studies. *J. Colloid Interface Sci.* **179**, 298–310 (1996).
34. Sabass, B., Gardel, M. L., Waterman, C. M. & Schwarz, U. S. High resolution traction force microscopy based on experimental and computational advances. *Biophys. J.* **94**, 207–20 (2008).
35. Döbereiner, H. G. *et al*. Lateral membrane waves constitute a universal dynamic pattern of motile cells. *Phys. Rev. Lett.* **97**, 10–13 (2006).
36. Barry, D. J., Durkin, C. H., Abella, J. V. & Way, M. Open source software for quantification of cell migration, protrusions, and fluorescence intensities. *J. Cell Biol.* **209**, 163–180 (2015).
37. Babu, A. R. & Gundiah, N. Role of Crosslinking and Entanglements in the Mechanics of Silicone Networks. *Exp. Mech.* **54**, 1177–1187 (2014).
38. Plotnikov, S. V, Sabass, B., Schwarz, U. S. & Waterman, C. M. High-resolution traction force microscopy. *Methods in cell biology* **123**, (Elsevier Inc., 2014).
39. Holenstein, C. N., Silvan, U. & Snedeker, J. G. High-resolution traction force microscopy on small focal adhesions - improved accuracy through optimal marker distribution and optical flow tracking. *Sci. Rep.* **7**, 41633 (2017).
40. Das, T., Maiti, T. K. & Chakraborty, S. Traction force microscopy on-chip: shear deformation of fibroblast cells. *Lab Chip* **8**, 1308–18 (2008).
41. Han, S. J., Oak, Y., Groisman, A. & Danuser, G. Traction microscopy to identify force modulation in subresolution adhesions. *Nat. Methods* **12**, 653–656 (2015).
42. Butler, J. P., Tolić-Nørrelykke, I. M., Fabry, B. & Fredberg, J. J. Traction fields, moments, and strain energy that cells exert on their surroundings. *Am. J. Physiol. Cell Physiol.* **282**, C595–605 (2002).
43. Kollmannsberger, P., Bidan, C. M., Dunlop, J. W. C. & Fratzl, P. The physics of tissue patterning and extracellular matrix organisation: how cells join forces. *Soft Matter* **7**, 9549–9560 (2011).
44. Balaban, N. Q. *et al*. Force and focal adhesion assembly: a close relationship studied using elastic micropatterned substrates. *Nat. Cell Biol.* **3**, 466–472 (2001).
45. Trichet, L. *et al*. Evidence of a large-scale mechanosensing mechanism for cellular adaptation to substrate stiffness. *Proc Natl Acad Sci USA* **108**, 6933–6938 (2012).
46. Shoham, N. & Gefen, A. The influence of mechanical stretching on mitosis, growth, and adipose conversion in adipocyte cultures. *Biomech. Model. Mechanobiol.* **11**, 1029–1045 (2012).
47. Na, S. *et al*. Rapid signal transduction in living cells is a unique feature of mechanotransduction. *Proc. Natl. Acad. Sci. USA* **105**, 6626–6631 (2008).
48. Goehring, N. W. & Grill, S. W. Cell polarity: Mechanochemical patterning. *Trends in Cell Biology* **23**, 72–80 (2013).
49. Khademolhosseini, F. Magnetically actuated microstructured surfaces can actively modify cell migration behaviour. *Biomed. Microdevices* 1–11, https://doi.org/10.1007/s10544-016-0033-7 (2016).
50. Segerer, F. J. *et al*. Versatile method to generate multiple types of micropatterns. *Biointerphases* **11**, 11005 (2016).


## Acknowledgements

This work was funded by the Agence Nationale de la Recherche (ANR, grant n° ANR-13-PDOC-0022-01), and supported by the CNRS and the Université Grenoble Alpes (UGA, AGIR-POLE program 2015, project ACTSUB). The authors are grateful to Dr. H. Maiato (University of Porto) for providing the NIH3T3 cells, to Dr. K. Miroshnikova (IAB, Grenoble) and K. Hennig (LIPhy, Grenoble) for the stable transfection with Vinculin-eGFP, Dr. S. Lecuyer and Dr. C. Verdier for their help with the rheology measurements and discussions, and finally the team of C. Albiges-Rizo (IAB, Grenoble) and D. Riveline (IGBMC, Université de Strasbourg) for support and fruitful discussions. C.M.B., A.C., M.B., T.B. and A.D. are part of the GDR 3070 CellTiss. Deep RIE was carried out at the PTA-Grenoble cleanroom facility. The authors are grateful to R. Haettel and J.-F. Motte of Institut NEEL for the development of a custom built substrate holder for the sputtering system and for FIB cutting, respectively.

## Author Contributions

M.B. and A.D. contributed to the concept of the magneto-active substrates. C.B., P.M., N.D., T.D., and A.D. designed the experimental setup. M.F., N.D., T.D. implemented the magneto-mechanical models and generated the numerical data. T.D. produced and characterized the magnetic templates and pillars. C.B. established the protocols, C.B. and A.L. performed the experiments. C.B. and T.B. performed the mechanical characterisation. C.B., A.C., A.L., I.W. and A.D. contributed to the data analysis. C.B., M.F., N.D., T.D. and A.D. drafted the work. All authors approved the final version of the manuscript.

## Additional Information

**Supplementary information** accompanies this paper at https://doi.org/10.1038/s41598-018-19804-1.

**Competing Interests:** The authors declare that they have no competing interests.

**Publisher's note:** Springer Nature remains neutral with regard to jurisdictional claims in published maps and institutional affiliations.